Journal of Solid Mechanics Vol. 17, No. 3 (2025) pp. 223-244
DOI: 10.60664/jsm.2025.1198459

Research Paper

Three Dimensional Thermo-Mechanical Bending Analysis of Multi-Directional Functionally Graded Annular Sector Plates Via GDQ Method

M. Adineh*, S.A.H. Sabzevari

Department of Mechanical Engineering, University of Gonabad, Gonabad, Iran

Received 3 February 2025; Received in revised form 28 September 2025; Accepted 30 October 2025

ABSTRACT

Banding analysis of functionally graded annular sector plates utilizing three-dimensional elasticity theory is the focus of this study. The equilibrium equations are derived based on three-dimensional elasticity theory and discretized using Generalized Differential Quadrature (GDQ) method. In this analysis, all material properties, except for the Poisson ratio, are assumed to vary along all three axes of cylindrical coordinates. Furthermore, all of them, except for the thermal conductivity coefficient, can be defined as temperature-dependent. To validate the method used, several examples were conducted in accordance with published results in the literature. Additionally, in some cases, due to a lack of data for the geometry under study, the results were compared with those obtained from the analysis of rectangular plates by increasing the ratio of the smaller radius to the larger one, which showed good agreement. The study investigates deflections and stresses at specified points on the plate under various boundary conditions, types of material gradation, and parameters related to the elastic foundation. The findings indicated that changes in the material composition of the plate along different directions of cylindrical coordinates can significantly affect the deformation and stress levels experienced by the plate.

Keywords: Annular sector plates*;* Multi-directional functionally graded plates*;* Three-dimensional thermo-elasticity*;* Elastic foundation.

1 INTRODUCTION

FUNCTIONALLY graded materials have been the subject of extensive research in the field of plate bending analysis over the past few decades [1]. Among these studies, annular sector plates represent a significant area of

*Corresponding author.
E-mail address: mahdi.adineh@gonabad.ac.ir (M. Adineh)

interest within this domain. Jomehzadeh et al. [2] presented an exact analytical method for the bending analysis of functionally graded (FG) annular sector plates. The governing equilibrium equations are derived using the first-order shear deformation plate theory. Saeidi et al. [3] presented an exact Levy-type solution for the bending analysis of a functionally graded (FG) annular sector plate. The governing equilibrium equations are derived using the classical plate theory framework. Fallah and Nosier [4] reformulated the governing equations of the first-order theory. This approach yields closed-form solutions for analyzing functionally graded circular sector plates. Karimi and Fallah [5] analyzed the nonlinear response of functionally graded (FG) sandwich circular sector plates with simply supported radial edges subjected to transverse loading using the first-order shear deformation theory, incorporating von Karman geometric nonlinearity. The governing equations are reformulated and solved through a combination of the single-parameter perturbation technique and Fourier series approaches. Aghdam et al. [6] introduced an iterative approach based on extended Kantorovich method (EKM) and First Order Shear Deformation Theory (FSDT) to obtain highly accurate solutions for the bending analysis of moderately thick, fully clamped functionally graded (FG) sector plates. Golmakani and Kadkhodayan [7] examined the large deflection behavior of stiffened annular functionally graded (FG) sector plates subjected to mechanical and thermo-mechanical loads. Utilizing the first-order shear deformation plate theory (FSDT) and von Karman relations for large deflections, nonlinear equilibrium equations are formulated. To solve these equations, the dynamic relaxation (DR) numerical method is employed in conjunction with the finite difference discretization technique. Golmakani and Alamatian [8] focused on the nonlinear bending behavior of moderately thick radially functionally graded (RFG) solid/annular sector plates resting on a two-parameter elastic foundation. The nonlinear formulations are derived using the first-order shear deformation theory (FSDT), incorporating the von Karman theory for large deflections and accounting for the interaction between the plate and the foundation. To solve the equilibrium equations, the dynamic relaxation (DR) method is utilized in conjunction with the finite difference discretization technique. Fereidoon et al. [9] derived The small deflection equation for an isotropic and non-homogeneous thin annular sector under transverse loading using polar coordinates. A closed-form solution with a fast convergence rate is achieved through the application of the extended Kantorovich method, alongside the classical thin plate theory (Kirchhoff theory). Alinaghizadeh and Shariati [10] examined the non-linear bending behavior of variable thickness two-directional functionally graded circular and annular sector plates supported by a non-linear elastic foundation. The analysis is conducted using the generalized differential quadrature (GDQ) method combined with the Newton–Raphson iterative approach. Alinaghizadeh and Shariati [11] explored the bending behavior of two-directional functionally graded circular and annular sector plates with variable thickness, both fully and partially supported by elastic foundations. Utilizing the first-order shear deformation theory and the concept of the physical neutral surface, the governing equations are formulated. To solve the resulting set of partial differential equations, a polynomial-based generalized differential quadrature method is applied. Mousavi and Tahani [12] introduced an analytical solution for the bending analysis of radially functionally graded (RFG) sector plates using the multi-term extended Kantorovich method (MTEKM). the governing equations are formulated based on first-order shear deformation theory and the state-space method is employed to solve the derived ODEs analytically. Alinaghizadeh and Kadkhodayan [13] explored the large deflection behavior of moderately thick radially functionally graded (RFG) annular sector plates, which are either fully or partially supported on a two-parameter Pasternak elastic foundation. The analysis is conducted using the Generalized Differential Quadrature (GDQ) method. The equilibrium equations are formulated based on the first-order shear deformation theory combined with non-linear von Kármán assumptions. Alinaghizadeh and Kadkhodayan [14] focused on the large deflection analysis of functionally graded annular sector plates under combined thermo-mechanical loading. Utilizing the first-order shear deformation theory and incorporating nonlinear von Kármán assumptions, the governing equations are formulated. These nonlinear equations are discretized using a polynomial-based generalized differential quadrature (GDQ) method. To solve the resulting system of nonlinear algebraic equations, the Newton-Raphson algorithm is applied. Fallah and Karimi [15] derived the nonlinear equilibrium equations for sector plates using the first-order shear deformation plate theory combined with von Karman strain-displacement relations. Through the decoupling of these equations, an analytical solution for the nonlinear behavior of functionally graded (FG) sector plates with simply-supported radial edges is achieved using the perturbation technique and the Fourier series method. Fallah and Khakbaz [16] Utilizing the first-order shear deformation plate theory, introduced two approaches within the framework of the extended Kantorovich method (EKM) for analyzing the bending behavior of functionally graded annular sector plates. In these approaches, the system of ordinary differential equations is addressed using the generalized differential quadrature method and the state space method. Kadkhodayan and Golmakani [17] examined the nonlinear bending behavior of solid and annular functionally graded (FG) sector plates under transverse mechanical loading and a thermal gradient along the thickness direction. Utilizing von-Kármán relations for large deflections, the nonlinear equilibrium equations are formulated based on first-order shear deformation theory (FSDT) and classical plate theory (CPT). To solve these

equations, the dynamic relaxation (DR) method is applied in combination with the finite difference discretization technique.

Although there of a lot of papers in which different plate theories have been used, many rare published papers deal with three dimensional elasticity theory. Zafarmand and Kadkhodayan [18] explored the three-dimensional static and dynamic behavior of a thick sector plate composed of two-directional functionally graded materials. The governing equations are derived using the 3D theory of elasticity. to solve these equations, the 3D graded finite element method (GFEM) is utilized. Asemi et al. [19] examined the three-dimensional static and dynamic analyses of two-dimensional functionally graded annular sector plates. The study employs graded finite element methods along with the Newmark direct integration technique to address the 3D elasticity equations within both spatial and temporal domains. Livani [20] focused on the three-dimensional bending analysis of a multi-directional functionally graded annular sector plate under transverse mechanical loading for a plate with clamped boundary conditions on all its edges. The governing and boundary equations are formulated using the three-dimensional theory of elasticity. To discretize and solve these equations, the differential quadrature method is applied. Niaraki et al. [21] developed a numerical solution for a circular section made of functionally graded material (FGM), with simply supported boundary conditions on the radial edges and subjected to a transverse load applied along the thickness. This analysis utilized the first-order shear deformation theory and the principle of minimum energy to achieve their results.

Multi-directional functionally graded plates with various geometries have been the focus of extensive research in recent years due to their applications and the potential to use material variation parameters to control the behavior of the plates [22-25]. Some of these papers have examined the effect of elastic foundation under conditions without temperature effects [26] or by considering temperature effects [27], which can help explore more diverse scenarios and also bring the results closer to real-world conditions.

Based on the best knowledge of the authors the bending of multi-directional functionally graded annular sector plates on an elastic foundation under mechanical and thermal loading has not been previously addressed. This research focuses on this issue for the first time. Three-dimensional elasticity theory has been used to derive the equations and GDQ is utilized to discretize them. The differential quadrature method (GDQ) is a numerical solution technique pioneered by the late Richard Bellman and his collaborators in the early 1970s. Since its development, this method has been effectively applied to a wide range of problems in engineering and the physical sciences [28]. The effects of boundary conditions, elastic foundation parameters, and material distribution have been considered for the plate under mechanical and thermal loads.

2 GEMETRY AND MATERIAL DISTRIBUTIONS

The plate under investigation in this study is an annular sector plate, along with its dimensional parameters, as shown in Fig. 1.

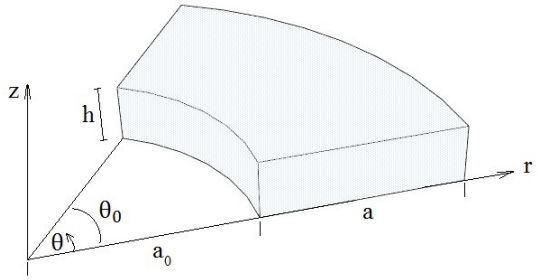

Fig. 1
Dimension parameters for the annular sector plate.

To simulate an annular sector plate, the equations of elasticity can be utilized in cylindrical coordinates. The relevant relationships are as follows.

Strain-Displacement Relations in Cylindrical Coordinates:

$$
\begin{aligned}
&\varepsilon_{\mathrm{r}}=\frac{\partial \mathrm{u}_{\mathrm{r}}}{\partial \mathrm{r}}\\
&\varepsilon_{\mathrm{r}\theta}=\frac{1}{2}\left(\frac{1}{\mathrm{r}}\frac{\partial \mathrm{u}_{\mathrm{r}}}{\partial \theta}+\frac{\partial \mathrm{u}_{\theta}}{\partial \mathrm{r}}-\frac{\mathrm{u}_{\theta}}{\mathrm{r}}\right)\\
&\varepsilon_{\mathrm{rz}}=\frac{1}{2}\left(\frac{\partial \mathrm{u}_{\mathrm{r}}}{\partial \mathrm{z}}+\frac{\partial \mathrm{u}_{\mathrm{z}}}{\partial \mathrm{r}}\right)\\
&\varepsilon_{\theta}=\frac{1}{\mathrm{r}}\frac{\partial \mathrm{u}_{\theta}}{\partial \theta}+\frac{\mathrm{u}_{\mathrm{r}}}{\mathrm{r}}\\
&\varepsilon_{\theta\mathrm{z}}=\frac{1}{2}\left(\frac{\partial \mathrm{u}_{\theta}}{\partial \mathrm{z}}+\frac{1}{\mathrm{r}}\frac{\partial \mathrm{u}_{\mathrm{z}}}{\partial \theta}\right)\\
&\varepsilon_{\mathrm{z}}=\frac{\partial \mathrm{u}_{\mathrm{z}}}{\partial \mathrm{z}}
\end{aligned}
\tag{1}
$$

Stress-Strain Relations in Cylindrical Coordinates:

$$
\begin{aligned}
&\varepsilon_{\mathrm{r}}=\frac{1}{\mathrm{E}}\left[\sigma_{\mathrm{r}}-\nu\left(\sigma_{\theta}+\sigma_{\mathrm{z}}\right)\right]+\alpha\Delta\mathrm{T}\\
&\varepsilon_{\theta}=\frac{1}{\mathrm{E}}\left[\sigma_{\theta}-\nu\left(\sigma_{\mathrm{r}}+\sigma_{\mathrm{z}}\right)\right]+\alpha\Delta\mathrm{T}\\
&\varepsilon_{\mathrm{z}}=\frac{1}{\mathrm{E}}\left[\sigma_{\mathrm{z}}-\nu\left(\sigma_{\mathrm{r}}+\sigma_{\theta}\right)\right]+\alpha\Delta\mathrm{T}\\
&\tau_{\mathrm{r}\theta}=\mathrm{G}\gamma_{\mathrm{r}\theta},\ \tau_{\mathrm{rz}}=\mathrm{G}\gamma_{\mathrm{rz}},\tau_{\theta\mathrm{z}}=\mathrm{G}\gamma_{\theta\mathrm{z}}
\end{aligned}
\tag{2}
$$

Equilibrium Equations in the Absence of Body Forces in Cylindrical Coordinates:

$$
\begin{aligned}
&\frac{\partial \sigma_{\mathrm{r}}}{\partial \mathrm{r}}+\frac{1}{\mathrm{r}}\frac{\partial \sigma_{\mathrm{r}\theta}}{\partial \theta}+\frac{\partial \sigma_{\mathrm{rz}}}{\partial \mathrm{z}}+\frac{\sigma_{\mathrm{r}}-\sigma_{\theta}}{\mathrm{r}}=0\\
&\frac{\partial \sigma_{\mathrm{r}\theta}}{\partial \mathrm{r}}+\frac{1}{\mathrm{r}}\frac{\partial \sigma_{\theta}}{\partial \theta}+\frac{\partial \sigma_{\mathrm{z}\theta}}{\partial \mathrm{z}}+\frac{2\sigma_{\mathrm{r}\theta}}{\mathrm{r}}=0\\
&\frac{\partial \sigma_{\mathrm{rz}}}{\partial \mathrm{r}}+\frac{1}{\mathrm{r}}\frac{\partial \sigma_{\theta\mathrm{z}}}{\partial \theta}+\frac{\partial \sigma_{\mathrm{z}}}{\partial \mathrm{z}}+\frac{\sigma_{\mathrm{rz}}}{\mathrm{r}}=0
\end{aligned}
\tag{3}
$$

To arrange the equations in a form suitable for discretization using the GDQ method, the equilibrium equations can be expressed in terms of displacement derivatives by combining relations 1 to 3. For example, the first equilibrium equation in relation 3 can be rewritten as shown in relation 4.

$$
\begin{aligned}
&\frac{\partial E}{\partial r}\frac{1}{(1+\nu)(1-2\nu)}\left[(1-\nu)\frac{\partial u_r}{\partial r}+\nu\left(\frac{1}{r}\frac{\partial u_\theta}{\partial \theta}+\frac{u_r}{r}\right)+\nu\frac{\partial u_z}{\partial z}\right]\\
&+\frac{E}{(1+\nu)(1-2\nu)}\left[(1-\nu)\frac{\partial^2 u_r}{\partial r^2}+\nu\left(\frac{-1}{r^2}\frac{\partial u_\theta}{\partial \theta}+\frac{1}{r}\frac{\partial^2 u_\theta}{\partial r\partial \theta}+\frac{1}{r}\frac{\partial u_r}{\partial r}-\frac{u_r}{r^2}\right)+\nu\frac{\partial^2 u_z}{\partial r\partial z}\right]\\
&-\frac{\partial E}{\partial r}\frac{\alpha\Delta T}{(1-2\nu)}-\frac{E}{(1-2\nu)}\frac{\partial \alpha}{\partial r}\Delta T-\frac{E}{(1-2\nu)}\alpha\frac{\partial(\Delta T)}{\partial r}+\frac{1}{2r}\frac{\partial E}{\partial \theta}\frac{1}{(1+\nu)}\left(\frac{1}{r}\frac{\partial u_r}{\partial \theta}+\frac{\partial u_\theta}{\partial r}-\frac{u_\theta}{r}\right)\\
&+\frac{1}{2r}\frac{E}{(1+\nu)}\left(-\frac{1}{r^2}\frac{\partial u_r}{\partial \theta}+\frac{1}{r}\frac{\partial^2 u_r}{\partial \theta^2}+\frac{\partial^2 u_\theta}{\partial r\partial \theta}+\frac{1}{r^2}u_\theta-\frac{1}{r}\frac{\partial u_\theta}{\partial \theta}\right)+\frac{1}{2}\frac{\partial E}{\partial z}\frac{1}{(1+\nu)}\left(\frac{\partial u_r}{\partial z}+\frac{\partial u_z}{\partial r}\right)+\frac{1}{2}\frac{E}{(1+\nu)}\left(\frac{\partial^2 u_r}{\partial z^2}+\frac{\partial^2 u_z}{\partial r\partial z}\right)\\
&+\frac{E}{(1+\nu)}\left[\frac{\partial u_r}{\partial r}-\frac{1}{r}\frac{\partial u_\theta}{\partial \theta}-\frac{u_r}{r}\right]=0
\end{aligned}
\tag{4}
$$

Temperature distribution in this study can be found from:

$$\frac{\partial}{\partial z}\left(\mathrm{K}\frac{\partial \mathrm{T}}{\partial \mathrm{z}}\right)=0 \tag{5}$$

where K represents the thermal conductivity coefficient. Boundary conditions used for edges in this study are:

$$\begin{aligned}
&\text{SSSS} \quad r=a_0,\ a_0+a \rightarrow \sigma_r=\ u_\theta=u_z=0\\
&\qquad \theta=0,\ \theta_0 \rightarrow \sigma_\theta=\ u_r=\ u_z=0\\
&\text{CCCC} \quad r=a_0,\ a_0+a \rightarrow\ u_r=\ u_\theta=\ u_z=0\\
&\qquad \theta=0,\ \theta_0 \rightarrow\ u_r=\ u_\theta=\ u_z=0\\
&\text{SCSC} \quad r=a_0,\ a_0+a \rightarrow \sigma_r=\ u_\theta=u_z=0\\
&\qquad \theta=0,\ \theta_0 \rightarrow\ u_r=\ u_\theta=\ u_z=0\\
&\text{CSCS} \quad r=a_0,\ a_0+a \rightarrow\ u_r=\ u_\theta=\ u_z=0\\
&\qquad \theta=0,\ \theta_0 \rightarrow \sigma_\theta=\ u_r=\ u_z=0
\end{aligned} \tag{6}$$

The boundary conditions used at the upper and lower surfaces of the plate are given by Eq.(7). The application of the elastic foundation to the model in this study is based on the boundary conditions applied at the underside surface of the plate. Coefficients K_{sr}, $K_{s\theta}$ and K_w are also the elastic foundation coefficients.

$$\begin{aligned}
&\sigma_z=q, \quad \sigma_{\mathrm{rz}}=\sigma_{\theta z}=0,\ T=T_u \quad at \quad z=h\\
&\sigma_z=K_w u_z-K_{sr}\frac{\partial^2 u_z}{\partial r^2}+K_{s\theta}\left(\frac{1}{r}\frac{\partial u_z}{\partial r}+\frac{1}{r^2}\frac{\partial^2 u_z}{\partial \theta^2}\right),\ \tau_{rz}=\ \tau_{\theta z}=0,\ T=T_l \quad at\ z=0
\end{aligned} \tag{7}$$

The material distribution used in this study is according to the following relation:

$$\begin{aligned}
&\mathrm{V_b}=\left(\frac{\mathrm{r}}{\mathrm{a}}\right)^{\mathrm{n_r}}\times\left(\frac{\theta}{\theta_0}\right)^{\mathrm{n_\theta}}\times\left(\frac{\mathrm{z}}{\mathrm{h}}\right)^{\mathrm{n_z}}\\
&\mathrm{P}=\mathrm{P_1}\left(1-\mathrm{V_b}\right)+\mathrm{P_2}\left(\mathrm{V_b}\right)
\end{aligned} \tag{8}$$

where P represent any material property of the plate. Additionally, the relationship between material properties and temperature is according to the following relation:

$$\mathrm{P}\left(\mathrm{T}\right)=\mathrm{Q_0}\left(\mathrm{Q_{-1}T^{-1}}+1+\mathrm{Q_1T}+\mathrm{Q_2T^2}+\mathrm{Q_3T^3}\right) \tag{9}$$

where the Q_i values are determined based on the material type.

3 NUMERICAL METHOD

In this study, the differential quadrature method is employed to discretize the equations outlined in the preceding section. When utilizing N nodal points for discretizing the parameter domain l, the *m-th* derivative of a function with respect to the parameter l is expressed in relation to the function values at all nodal points within that domain as follows:

$$\left.\frac{\mathrm{d^m f\left(x\right)}}{\mathrm{dl^m}}\right|_{\mathrm{n=n_i}}=\sum_{\mathrm{j=1}}^{\mathrm{N}}\mathrm{C_{ij}^{(m)}f\left(l_j\right)}, \qquad \mathrm{i}=1, 2, \ldots, \mathrm{N} \tag{10}$$

The weighting coefficients $C_{ij}^{(m)}$ in this equation are derived for the first derivative from Eq. (11) and for higher-order derivatives from Eq. (12).

$$C_{ij}^{(1)} = \frac{\prod_{j=1,j\neq i}^{N}\left(l_i - l_j\right)}{\left(l_i - l_k\right)\prod_{j=1,j\neq k}^{N}\left(l_k - l_j\right)}, \qquad i,\ j,\ k = 1, 2, \ldots,\ N$$
$$C_{ii}^{(1)} = -\sum_{j=1,j\neq i}^{N} C_{ij}^{1}, \qquad i = 1, 2, \ldots,\ N \tag{11}$$

$$C_{ij}^{(m)} = C_{ij}^{(1)} \times C_{ij}^{(m-1)} \tag{12}$$

To establish the distribution of domain points, a Chebyshev polynomial is utilized according to the specified equation.

This reformulation provides a robust framework for applying the differential quadrature method across various engineering and scientific problems, enhancing both accuracy and computational efficiency.

$$l_i = 0.5L\left(1 - \frac{\cos\left(i-1\right)\times\pi}{N-1}\right) \tag{13}$$

In the equation above, *L* represents the length of the domain.

4 VALIDATION

To ensure the accuracy of the results, several numerical experiments were conducted and compared with existing data published in the literature. The first validation pertains to the bending of a fully clamped annular sector plate subjected to a uniform compressive loading (q= 50 *KPa*), with the results presented in Table 1. The angle used for the sector is $\pi/3$ and the plate thickness is set at 0.002. mechanical properties are E=207*GPa* and ν =0.3.The deflection of the plate is non-dimensionalized using relation 14. As observed, especially for a higher number of nodal points, there is a satisfactory agreement between the obtained results, although the results also appear acceptable for fewer points. It is also observed that the discrepancies increase in thicker plates, which is likely due to the use of three-dimensional elasticity theory in the present study, providing more accuracy compared to the theory used in reference [29], which pertains to thin plates.

$$\bar{w} = Dw_{min} / q\left(a_0 + a\right)^4$$
$$D = Eh^3 / 12\left(1 - \nu^2\right) \tag{14}$$

Table 1
Maximum non-dimensionalized deflection of an annular sector plate under uniform loading.

$a_0/\left(a_0+a\right)$	a_0	a	$N_r \times N\theta \times N_z$	$\bar{w}$		
				GDQ	Ref [29]	Difference (%)
0.75	0.375	0.125	$7\times7\times7$	0.000010664	0.0000102	4.54902
			$9\times9\times9$	0.00001013	0.0000102	-0.68627
			$11\times11\times11$	0.000010254	0.0000102	0.529412
			$13\times13\times13$	0.000010244	0.0000102	0.431373
			$15\times15\times15$	0.000010238	0.0000102	0.372549
			$17\times17\times17$	0.000010235	0.0000102	0.343137
			$19\times19\times19$	0.000010236	0.0000102	0.352941
0.5	0.25	0.25	$7\times7\times7$	0.00013993	0.000142	-1.45775
			$9\times9\times9$	0.00013834	0.000142	-2.57746
			$11\times11\times11$	0.00014107	0.000142	-0.65493
			$13\times13\times13$	0.00014044	0.000142	-1.09859

			$15\times15\times15$	0.00014164	0.000142	-0.25352
			$17\times17\times17$	0.00014103	0.000142	-0.6831
			$19\times19\times19$	0.00014138	0.000142	-0.43662
0.25	0.125	0.375	$7\times7\times7$	0.00026805	0.000286	-6.27622
			$9\times9\times9$	0.00027292	0.000286	-4.57343
			$11\times11\times11$	0.0002757	0.000286	-3.6014
			$13\times13\times13$	0.00027509	0.000286	-3.81469
			$15\times15\times15$	0.00027797	0.000286	-2.80769
			$17\times17\times17$	0.00027825	0.000286	-2.70979
			$19\times19\times19$	0.00027976	0.000286	-2.18182

To validate the impact of the elastic foundation on the bending of the plate, and considering the scarcity of references that have examined annular sector plates, the size a_0 was increased relative to the size a, resulting in a geometry similar to that of a rectangular plate. This configuration was then compared with the reference [30]. material used in this case is according to Table 2. As shown in table 3, the agreement of results for varying values of K_0 and under conditions where $j_0 = 0$ is satisfactory. However, for values of $j_0 = 100$ there is a slight deviation in the results, which may likely be attributed to the minor differences arising from simulating an annular sector plate as a rectangular plate. In this example, the gradual variations of the material were also tested, showing good agreement. The parameters used in this section are:

a_0 =1000 *m*, a = 3 *m*, h =0.1 *m*, θ_0 =0.001 *rad*, q=10^3*Pa*

Table 2
Material properties.

Material property	value
Em	70 *GPa*
ν_m	0.3
Ec	380 *GPa*
ν_c	0.3

Non-dimensional deformation and stresses used in Table 3 is according to below:

$$\sigma_r^* = -\frac{h^2}{qa^2}\sigma_r\left(\frac{a}{2},\frac{a_0\theta_0}{2},0\right)$$
$$\sigma_\theta^* = -\frac{h^2}{qa^2}\sigma_\theta\left(\frac{a}{2},\frac{a_0\theta_0}{2},0\right)$$
$$\sigma_{r\theta}^* = -\frac{h^2}{qa^2}\sigma_{r\theta}\left(0,0,0\right)$$
$$w^* = \frac{100D_0}{qa^4}w\left(\frac{a}{2},\frac{a_0\theta_0}{2},\frac{h}{2}\right) \quad (15)$$
$$D_0 = \frac{E_c h^3}{12\left(1-\nu^2\right)}$$
$$K_0 = \frac{K_w a^4}{E_0 h^3}$$
$$J_0 = \frac{K_{sr}b^2}{E_0h^3} = \frac{K_{s\theta}a^2}{E_0h^3}$$
$$E_0 = 1.0\ \text{GPa},\ \nu = 0.3$$

Table 3
Nondimensional deformation and stresses of a FGM rectangular plate on elastic foundation.

		K_0	J_0	$N_r \times N_\theta \times N_z$					ref [30]
				$7\times7\times7$	$9\times9\times9$	$11\times11\times11$	$13\times13\times13$	$15\times15\times15$	
n_z=0	w^*	0	0	1.2478	1.2616	1.2611	1.2608	1.2608	1.2583
	σ_r^*			0.7066	0.717	0.7171	0.7166	0.7169	0.716
	σ_θ^*			0.2317	0.247	0.2455	0.2451	0.2455	0.2447
	$\sigma_{r\theta}^*$			0.2671	0.2834	0.286	0.2866	0.2866	0.289
	w^*	100	0	1.2157	1.2293	1.2288	1.2285	1.2286	1.226
	σ_r^*			0.6875	0.6979	0.698	0.6975	0.6978	0.6969
	σ_θ^*			0.2244	0.2397	0.2383	0.2379	0.2382	0.2375
	$\sigma_{r\theta}^*$			0.2621	0.2785	0.2811	0.2816	0.2817	0.284
	w^*	0	100	1.1874	1.2007	1.2001	1.1998	1.1999	1.1662
	σ_r^*			0.6719	0.682	0.682	0.6815	0.6818	0.6618
	σ_θ^*			0.2216	0.2365	0.2348	0.2345	0.2349	0.2245
	$\sigma_{r\theta}^*$			0.2524	0.2681	0.2708	0.2713	0.2713	0.2744
	w^*	100	100	1.1583	1.1715	1.1709	1.1707	1.1707	1.1382
	σ_r^*			0.6547	0.6647	0.6647	0.6642	0.6645	0.6452
	σ_θ^*			0.215	0.2299	0.2282	0.2279	0.2283	0.2183
	$\sigma_{r\theta}^*$			0.2479	0.2636	0.2663	0.2669	0.2669	0.27
n_z=1	w^*	0	0	2.5066	2.526	2.5236	2.5231	2.5232	2.5134
	σ_r^*			0.3218	0.3254	0.3252	0.325	0.3251	0.325
	σ_θ^*			0.1056	0.112	0.1114	0.1112	0.1113	0.1111
	$\sigma_{r\theta}^*$			0.121	0.1279	0.1291	0.1293	0.1294	0.1306
	w^*	100	0	2.3809	2.4007	2.3984	2.3979	2.398	2.3875
	σ_r^*			0.3047	0.3084	0.3082	0.308	0.3081	0.308
	σ_θ^*			0.099	0.1055	0.1048	0.1046	0.1048	0.1047
	$\sigma_{r\theta}^*$			0.1166	0.1236	0.1248	0.125	0.125	0.1262
	w^*	0	100	2.2749	2.2942	2.2917	2.2914	2.2914	2.1703
	σ_r^*			0.2914	0.2948	0.2946	0.2944	0.2945	0.2791
	σ_θ^*			0.0965	0.1026	0.1018	0.1017	0.1018	0.094
	$\sigma_{r\theta}^*$			0.1084	0.1149	0.1161	0.1164	0.1164	0.1182
	w^*	100	100	2.1715	2.1911	2.1887	2.1884	2.1884	2.0746
	σ_r^*			0.2774	0.2808	0.2806	0.2804	0.2805	0.2663
	σ_θ^*			0.0911	0.0972	0.0964	0.0962	0.0964	0.0893
	$\sigma_{r\theta}^*$			0.1048	0.1114	0.1126	0.1129	0.1129	0.1148

Table 4 examines the sensitivity of the responses with respect to the number of nodal points in each coordinate direction. For this purpose, the first section of Table 3, which includes dimensionless displacements and stresses for the case (K_0=J_0=0) in an isotropic plate, has been analyzed. It is observed that within the studied range, the response sensitivity is highest in the r-direction, while increasing the number of nodal points in the circumferential and thickness directions, without changing the nodal points in other directions, does not significantly affect the responses.

Table 4
Sensitivity of results to the number of grid points (N_r, N_θ, N_z).

$N_r \times N_\theta \times N_z$	6 × 6 × 6	8 × 6 × 6	10 × 6 × 6	12 × 6 × 6	14 × 6 × 6	Ref [30]
w^*	1.2478	1.2618	1.2614	1.2613	1.2614	1.2583
σ_r^*	0.7066	0.717	0.7169	0.7165	0.7167	0.716
σ_θ^*	0.2317	0.247	0.2455	0.2452	0.2455	0.2447
$\sigma_{r\theta}^*$	0.2671	0.2826	0.2852	0.2859	0.2861	0.289
$N_r \times N_\theta \times N_z$	6 × 6 × 6	6 × 8 × 6	6 × 10 × 6	6 × 12 × 6	6 × 14 × 6	Ref [30]
w^*	1.2478	1.2475	1.2474	1.2473	1.2472	1.2583
σ_r^*	0.7066	0.7067	0.7068	0.7067	0.7068	0.716
σ_θ^*	0.2317	0.2316	0.2317	0.2316	0.2317	0.2447
$\sigma_{r\theta}^*$	0.2671	0.2677	0.2677	0.2677	0.2676	0.289
$N_r \times N_\theta \times N_z$	6 × 6 × 6	6 × 6 × 8	6 × 6 × 10	6 × 6 × 12	6 × 6 × 14	Ref [30]
w^*	1.2478	1.2478	1.2478	1.2478	1.2478	1.2583
σ_r^*	0.7066	0.7066	0.7066	0.7066	0.7066	0.716
σ_θ^*	0.2317	0.2317	0.2317	0.2317	0.2317	0.2447
$\sigma_{r\theta}^*$	0.2671	0.2671	0.2671	0.2671	0.2671	0.289

To ensure the accuracy of the results for thermal loading, the impact of this loading condition will also be examined. Due to the lack of suitable references addressing thermal loading on functionally graded plates with an annular sector geometry, a method similar to that used in the previous example was employed to compare the results with those of a rectangular plate from reference [31]. The deflection of the plate is presented in Table 6 and Fig. 2, demonstrating good agreement. A slight discrepancy may arise due to assuming a constant Poisson's ratio of 0.3 for all points on the plate. In this example, the upper surface of the plate is at temperature T=1000 and the lower surface is at temperature T=300. Additionally, the material properties, which are temperature-dependent, are specified in Table 5.

Table 5
The temperature-dependent material properties of Si3N4 and SUS304 [31].

Material	Property	Q_{-1}	Q_0	Q_1	Q_2	Q_3
Si_3N_4	$E(Pa)$	0	348.43×10^9	-3.07×10^{-4}	2.16×10^{-7}	-8.946×10^{-11}
	ν	0	0.24	0	0	0
	$\alpha(1/K)$	0	5.87×10^{-6}	9.095×10^{-4}	0	0
	$\rho(kg/m^3)$	0	2370	0	0	0
	$K(W/mK)$	0	9.19	0	0	0
	$c(J/kg\,K)$	0	0.17	0	0	0
SUS304	$E(Pa)$	0	201.04×10^9	3.079×10^{-4}	-6.534×10^{-7}	0
	ν	0	0.3262	-2.002×10^{-4}	3.797×10^{-7}	0
	$\alpha(1/K)$	0	12.33×10^{-6}	8.086×10^{-4}	0	0
	$\rho(kg/m^3)$	0	8166	0	0	0
	$K(W/mK)$	0	12.04	0	0	0
	$c(J/kgK)$	0	0.08	0	0	0

Table 6
Deflection of the plate at $(a + \frac{2_0}{2}, \frac{2_0\theta_0}{2}, h)$.

$N_r \times N_\theta \times N_z$	w (m)
7 × 7 × 7	0.007
9 × 9 × 9	0.0069
11 × 11 × 11	0.0068
13 × 13 × 13	0.0068
15 × 15 × 15	0.0067
17 × 17 × 17	0.0067

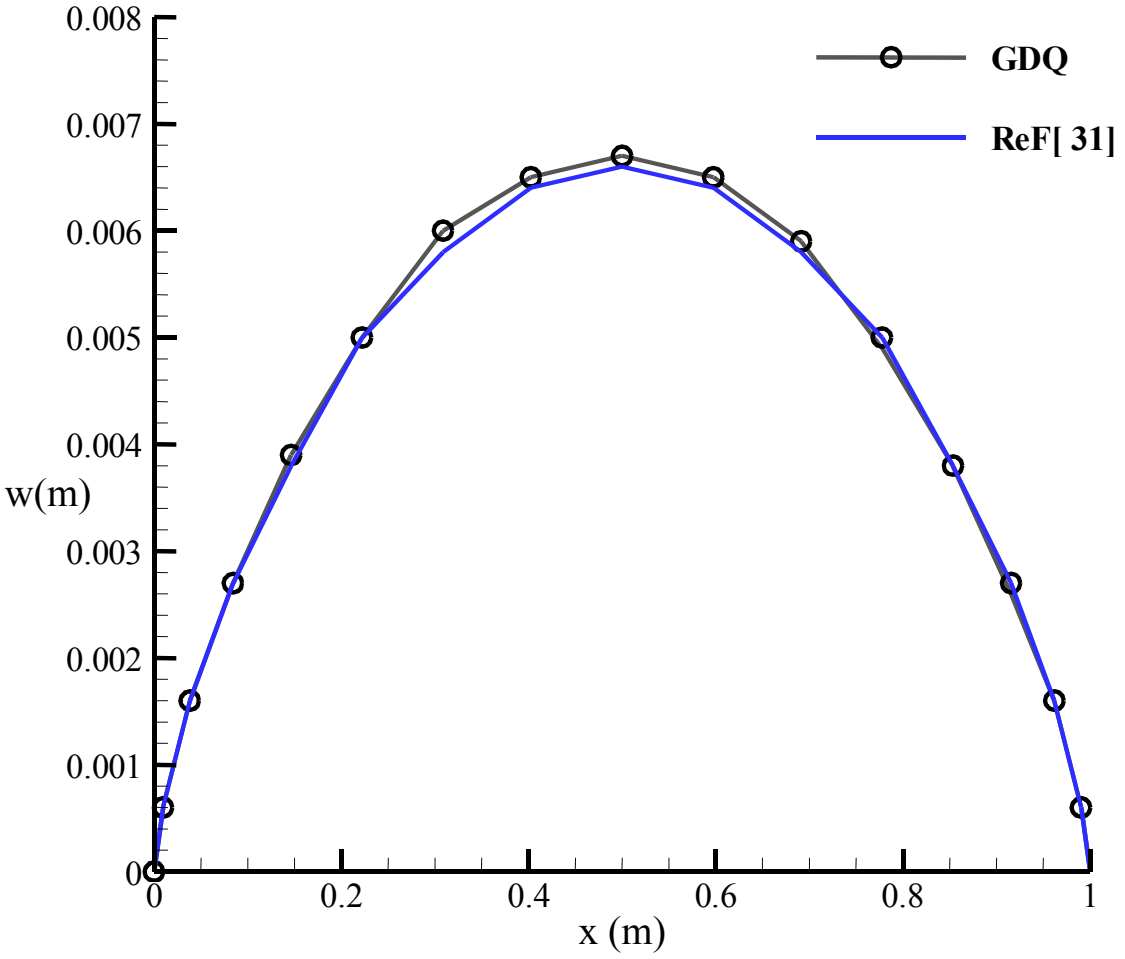

Fig.2

Deflection variation along the r direction at $\theta=\frac{2_0\theta_0}{2}$ and z=h.

5 RESULTS

In the following sections, we will examine the behavior of an annular sector plate under various conditions. In all cases considered, the material properties of the plate are consistent with those outlined in Table 2. Also the non-dimensional parameters are all consistent with the relationship 14.

Initially, the effect of gradual material variation in different directions of the cylindrical coordinates will be addressed. As illustrated in Fig. 3, it is observed that the material changes in the radial direction have the least impact on the deformation at the center of the plate. Furthermore, despite an initial opposing trend, the material variations in the circumferential direction ultimately exert a greater influence on the deformation at the center of the plate compared to those in the thickness direction. Notably, as shown in the Fig. 3, simultaneous gradual changes in material properties across all three coordinate directions generally have a more significant effect on the deformation shape at the center of the plate than changes in any single direction.

Additionally, referring to Figs. 4 and 5, it can be seen that the lowest radial and circumferential stresses at the examined point occur at lower powers of the material variation function related to functionally graded materials in the thickness direction. However, as the power of this function increases, these stresses gradually rise and approach those observed in other graphs. It is also noted that for both radial and circumferential stresses, the highest values at larger powers of the function pertain to three-dimensional functionally graded materials.

Considering Figs. 3, 4, and 5, it can be concluded that despite fluctuations at lower powers of the material variation function, at higher powers, the graphs exhibit a more uniform and stable behavior. This may be attributed to an increase in one of the material phases dominating the bending behavior of the plate.

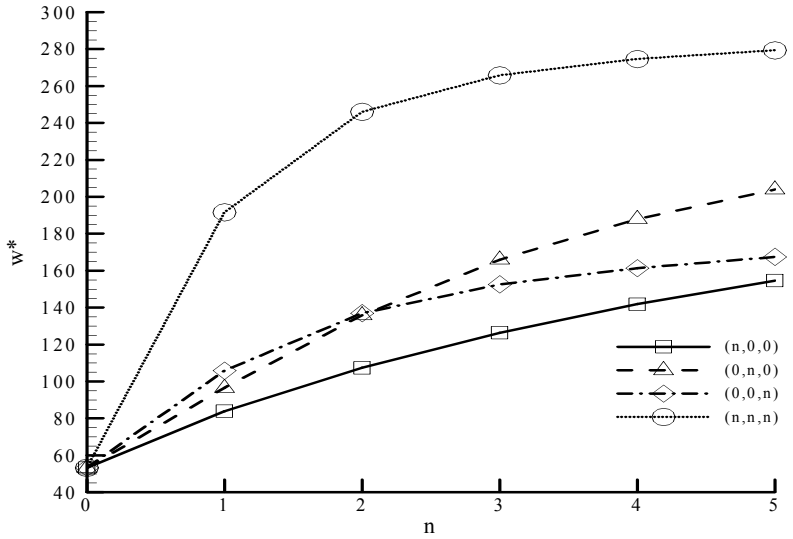

Fig.3
The effect of material distribution function powers on non-dimensional deformation w*. ($a_0 = 0.2$, a = 0.8, $\theta_0 = \pi / 3$, z = 0.1, $q=10^3$, $K_0 = J_0 = 0$, $Tu = T_1 = 0$, SSSS).

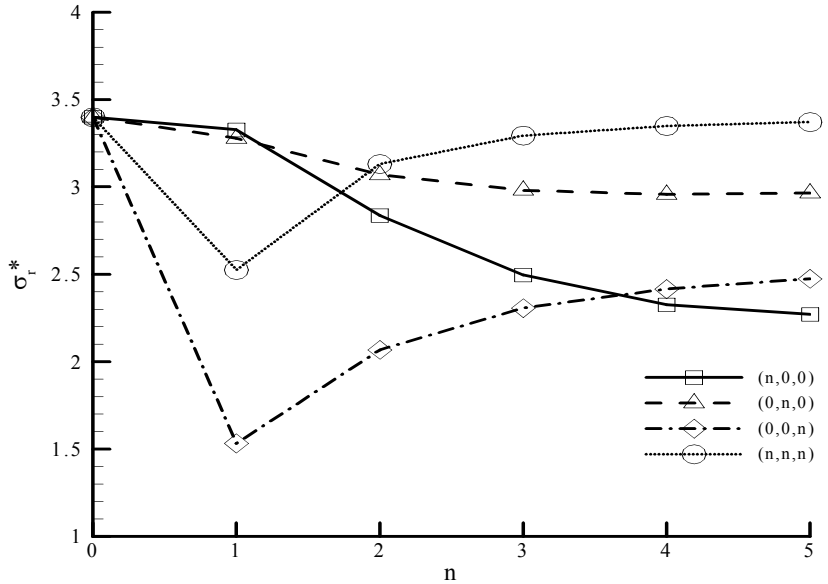

Fig.4
The effect of material distribution function powers on non-dimensional stress σ_r^*. ($a_0 = 0.2$, a = 0.8, $\theta_0 = \pi / 3$, z = 0.1, $q = 10^3$, $K_0 = J_0 = 0$, $Tu = T_1 = 0$, SSSS).

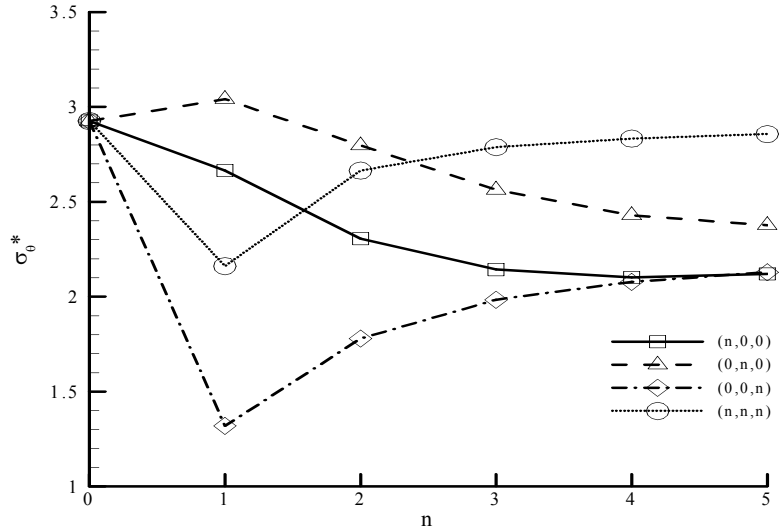

Fig.5

The effect of material distribution function powers on non-dimensional stress σ_θ^* . (a_0 =0.2, a =0.8, $\theta_0 = \pi / 3$, z =0.1, q=10^3, $K_0 = J_0 = 0$,Tu =T_1=0, SSSS).

In the subsequent sections, the plate subjected to thermal loading will be examined. In this plate, the temperatures of the upper and lower surfaces are set at 300°C and 0°C, respectively. As shown in Fig. 6, the maximum and minimum deformations correspond to the three-dimensional functionally graded plate and the functionally graded plate in the thickness direction.

As observed in Figs. 7 and 8, the effect of increasing the power of the function on radial and circumferential stresses is nearly similar for all four types of plates, although the magnitude of the effect varies.

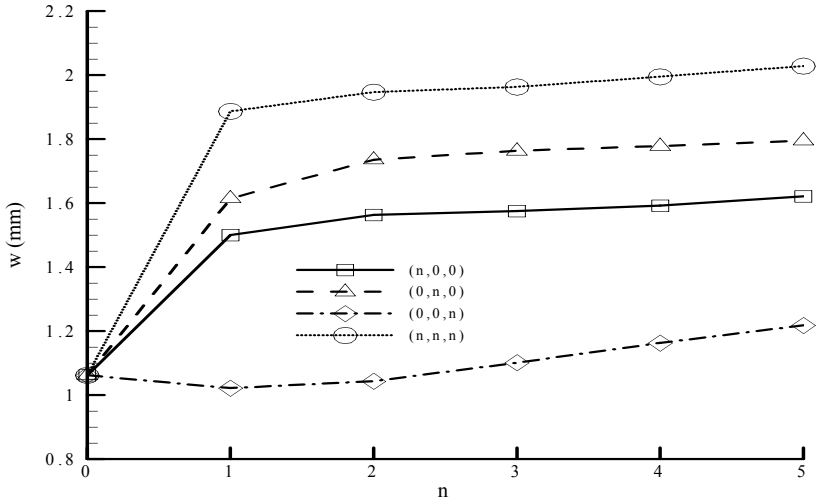

Fig.6

The effect of material distribution function powers on non-dimensional deflection w. (a_0 = 0.2, a = 0.8, $\theta_0 = \pi / 3$, z = 0.1, q = 0, $K_0 = J_0 = 0$,Tu = 300,T_1= 0, SSSS).

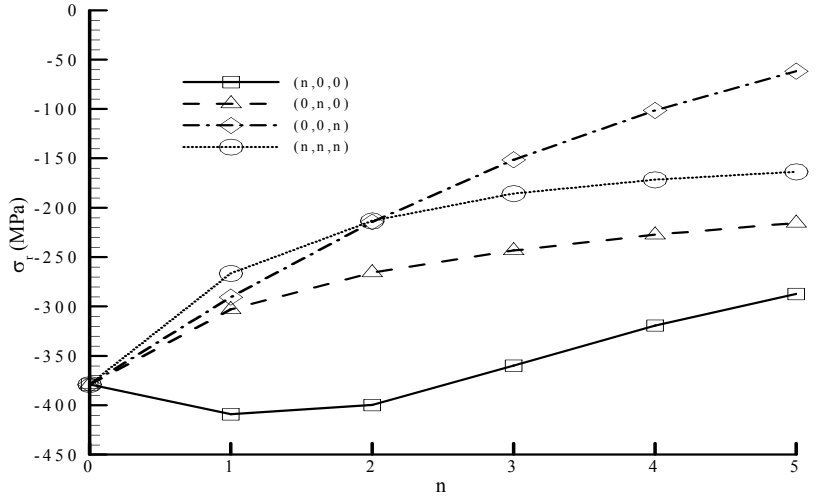

Fig.7
The effect of material distribution function powers on non-dimensional stress σ_r . ($a_0 = 0.2$, a = 0.8, $\theta_0 = \pi / 3$, z = 0.1, q = 0, $K_0 = J_0 = 0$,Tu = 300,$T_1 = 0$, SSSS).

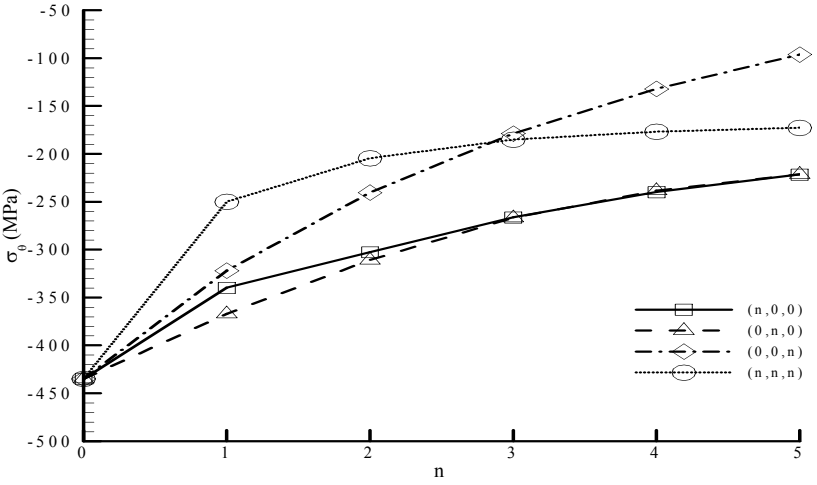

Fig.8
The effect of material distribution function powers on non-dimensional stress σ_θ . ($a_0 = 0.2$, a = 0.8, $\theta_0 = \pi / 3$, z = 0.1, q = 0 , $K_0 = J_0 = 0$,Tu = 300,$T_1 = 0$, SSSS).

In the following sections, the impact of the elastic foundation on the plate under compressive loading is examined. As shown in Fig. 9, the presence of the elastic foundation with any coefficient K_0 and J_0 can reduce the deformation of all five types of plates, with an increase in K_0 proving to be more effective than J_0. The elastic foundation does not alter the relative positions of the different plates, meaning that, for instance, the 3D functionally graded plate in all elastic foundation coefficients examined exhibits greater deformation compared to the other plates.

Additionally, the presence of the elastic foundation results in a decrease in radial and circumferential stress values at the examined point across all plates, with an increase in K_0 being more effective than J_0. This effect may be attributed to the reduced bending of the plate and the associated stresses.

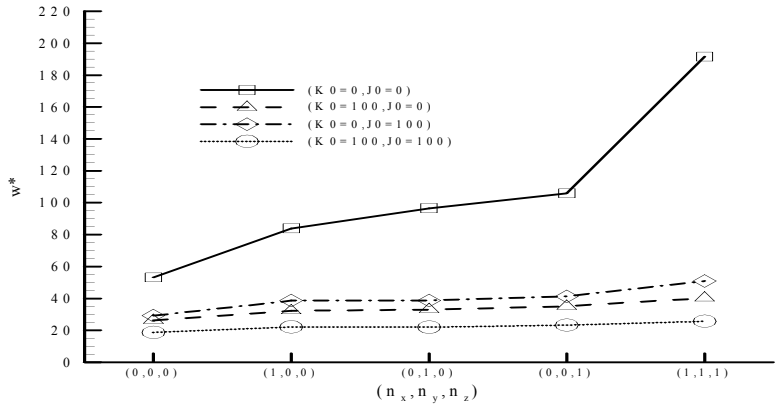

Fig.9
The effect of elastic foundation on non-dimensional deflection w*. ($a_0 = 0.2$, a = 0.8, $\theta_0 = \pi / 3$, z = 0.1, q = 10^3,Tu = T_1 = 0, SSSS).

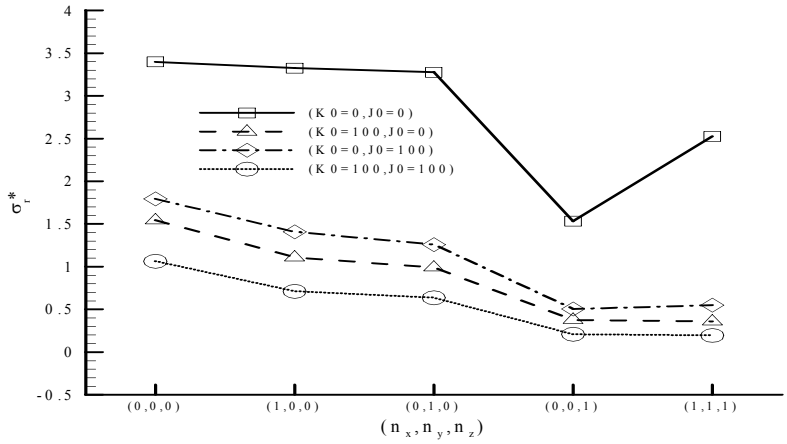

Fig.10
The effect of elastic foundation on non-dimensional stress σ_r^* . ($a_0 = 0.2$, a = 0.8, $\theta_0 = \pi / 3$, z = 0.1, q =1 0^3 ,Tu = T_1 = 0, SSSS).

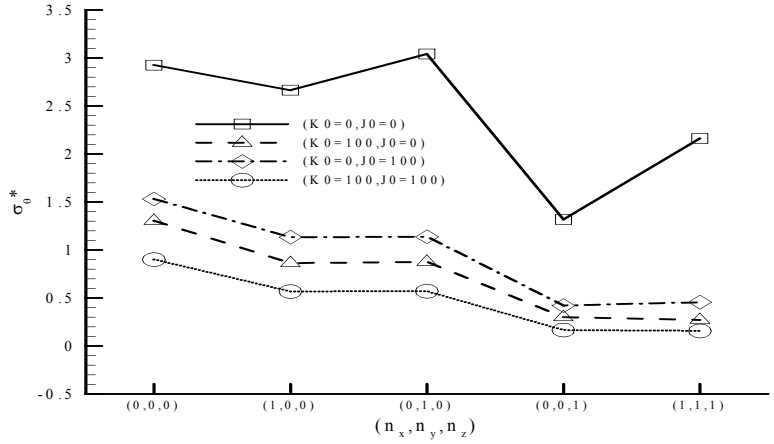

Fig.11
The effect of elastic foundation on non-dimensional stress σ_θ^* . ($a_0 = 0.2$, a = 0.8, $\theta_0 = \pi / 3$, z = 0.1, q = 10^3, Tu = T_1 = 0, SSSS).

Figs. 12 to 14 illustrate that the influence of the elastic foundation parameters on the plate's response under thermal loading is similar to that under mechanical loading. However, for thermal loading, the parameter J_0 exhibits a more significant effect compared to K_0. This observation may be attributed to the different deformation behaviors

of the plate under mechanical and thermal loading. In thermal loading, in addition to bending in one direction, the points on the plate tend to increase their separation due to thermal expansion caused by the rise in temperature.

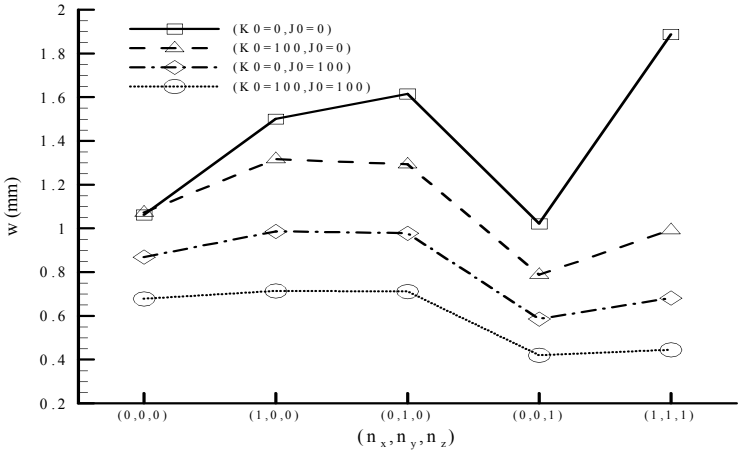

Fig.12
The effect of elastic foundation on the deflection w. ($a_0 = 0.2$, a = 0.8, $\theta_0 = \pi / 3$, z = 0.1, q = 0,Tu = 300, $T_1 = 0$, SSSS).

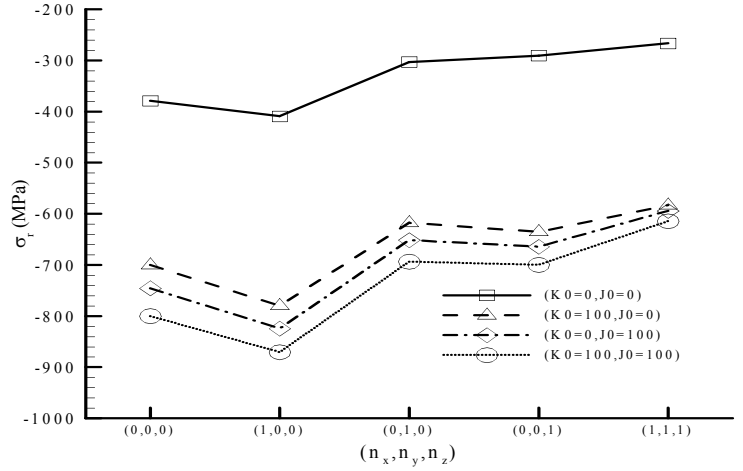

Fig.13
The effect of elastic foundation on the stress σ_r . ($a_0 = 0.2$, a = 0.8, $\theta_0 = \pi / 3$, z = 0.1, q = 0 ,Tu = 300, $T_1 = 0$, SSSS).

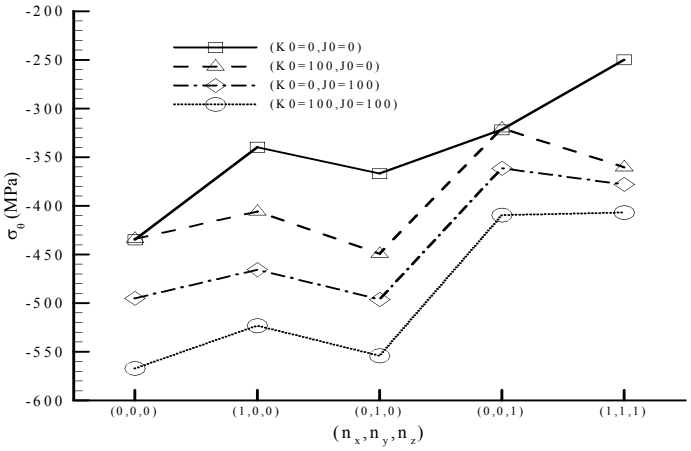

Fig.14
The effect of elastic foundation on the stress σ_θ . ($a_0 = 0.2$, a = 0.8, $\theta_0 = \pi / 3$, z = 0.1, q = 0, Tu = 300, $T_1 = 0$, SSSS).

Based on Figs. 15, 16, and 17, increasing the angle of the sector leads to a reduction in the deformation at the center of the plate and radial stress at the examined point; however, the trend for circumferential stress shows a different pattern.

By comparing Figs. 15 to 17 with Figs. 18 to 20, it can be observed that the effect of increasing the angle of the sector on the response of the plate under thermal loading differs from its response under mechanical loading.

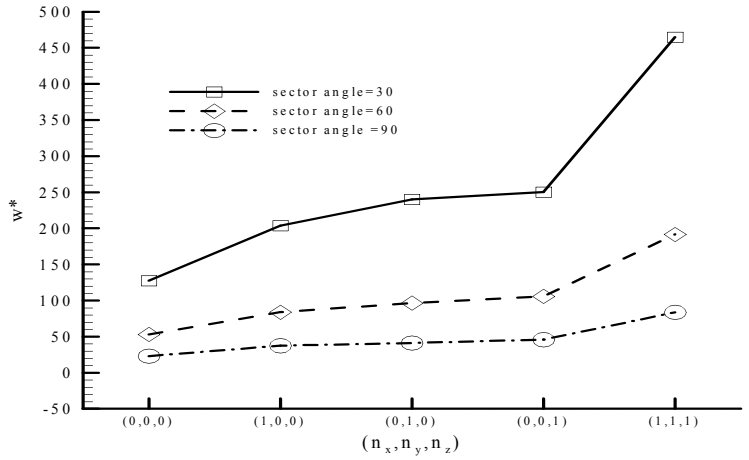

Fig.15
The effect of sector angle on non-dimensional deflection w*. ($a_0 = 0.2$, a = 0.8, z = 0.1, $q = 10^3$, $K_0 = J_0 = 0$, $Tu = T_1 = 0$, SSSS).

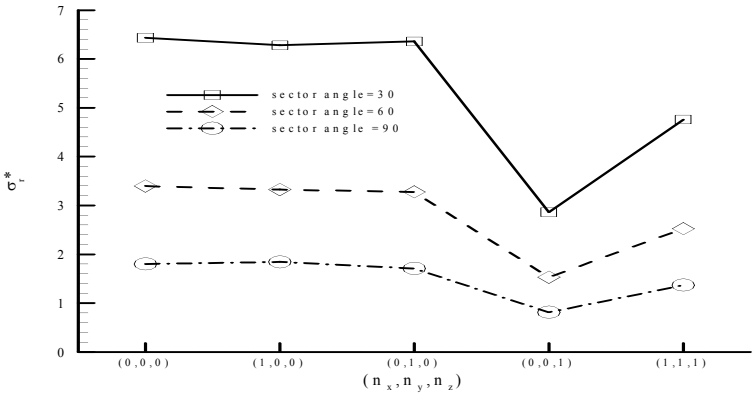

Fig.16
The effect of sector angle on non-dimensional stress σ_r^*. ($a_0 = 0.2$, a = 0.8, z = 0.1, $q = 10^3$, $K_0 = J_0 = 0$, $Tu = T_1 = 0$, SSSS).

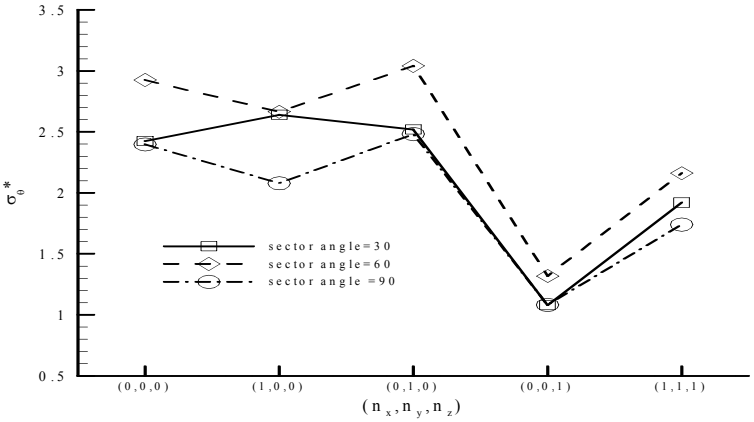

Fig.17
The effect of sector angle on non-dimensional stress σ_θ^*. ($a_0 = 0.2$, a = 0.8, z = 0.1, $q = 10^3$, $K_0 = J_0 = 0$, $Tu = T_1 = 0$, SSSS).

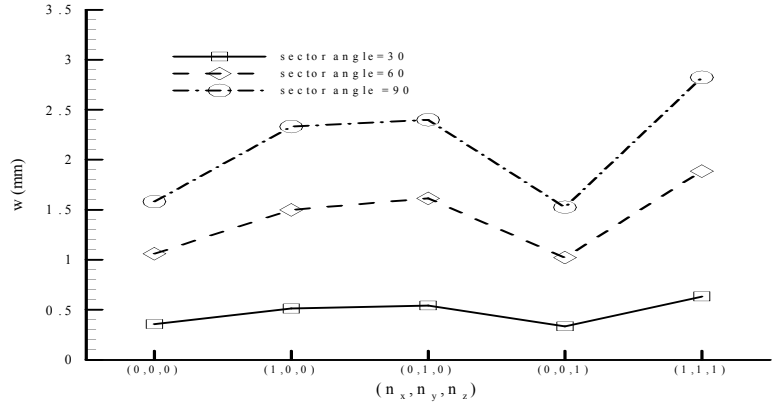

Fig.18
The effect of sector angle on the deflection w. ($a_0 = 0.2$, a = 0.8, z = 0.1, q = 0, $K_0 = J_0 = 0$, Tu = 300, $T_1 = 0$, SSSS).

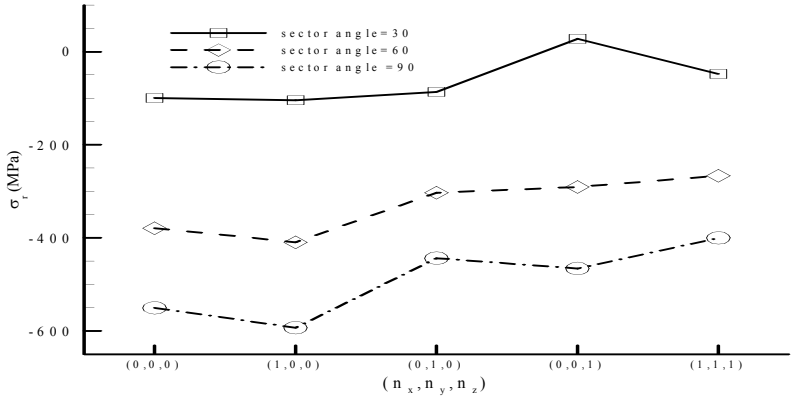

Fig.19
The effect of sector angle on the stress σ_r . ($a_0 = 0.2$, a = 0.8, z = 0.1, q = 0, $K_0 = J_0 = 0$, Tu = 300, $T_1 = 0$, SSSS).

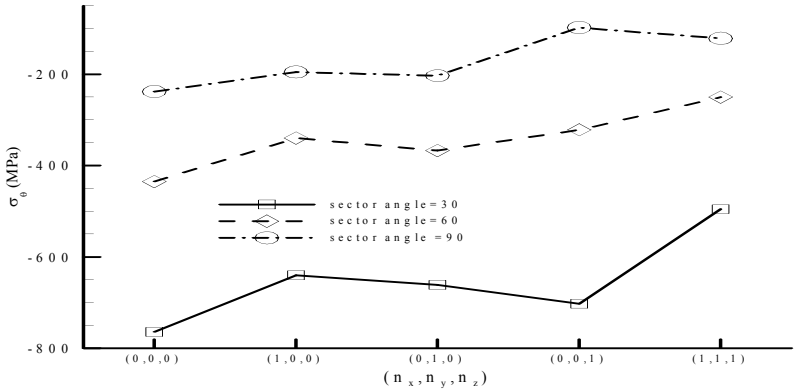

Fig.20
The effect of sector angle on non-dimensional stress σ_θ . ($a_0 = 0.2$, a = 0.8, z = 0.1, q = 0, $K_0 = J_0 = 0$, Tu = 300, $T_1 = 0$, SSSS).

Figs. 21 to 26 illustrate that the maximum and minimum deformations occur for the boundary conditions SSSS and CCCC, respectively, in both mechanical and thermal load cases, which is predictable given the more constrained nature of the clamped boundary conditions. Additionally, the positions of the SCSC and CSCS boundary conditions indicate that in the plate under mechanical load, the boundary conditions on the curved edges have a greater influence on the plate's behavior compared to the other two edges, Conversely, for the plate under thermal loading, the opposite behavior is observed.

Furthermore, as observed in Figs. 21 to 26, the boundary conditions have an overall effect on all types of plates, and they do not significantly alter the influence of material variation direction. Specifically, under all support

conditions, the greatest deformation consistently corresponds to (1,1,1), remaining unchanged with varying boundary conditions.

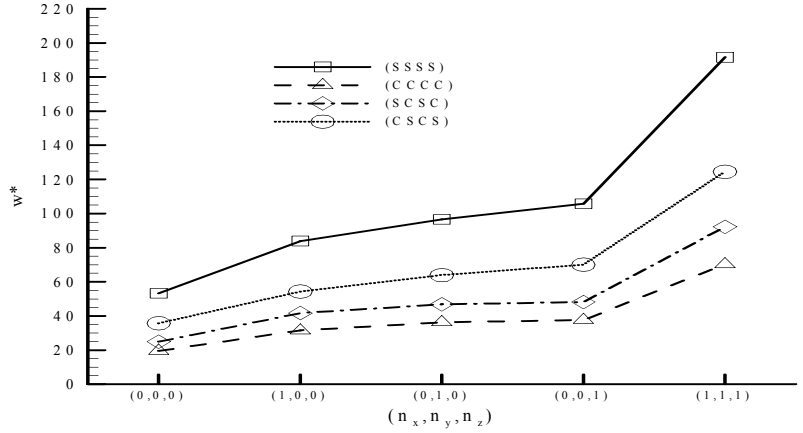

Fig.21
The effect of boundary conditions on non-dimensional deflection w*. ($a_0 = 0.2$, a = 0.8, $\theta_0 = \pi / 3$, z = 0.1, $q = 10^3$, $K_0 = J_0 = 0$, $Tu = T_1 = 0$).

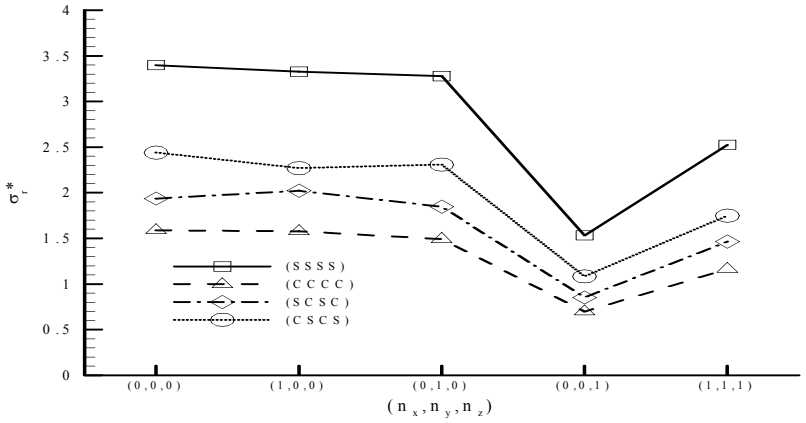

Fig.22
The effect of boundary conditions on non-dimensional stress σ_r^*. ($a_0 = 0.2$, a = 0.8, $\theta_0 = \pi / 3$, z = 0.1, $q = 10^3$, $K_0 = J_0 = 0$, $Tu = T_1 = 0$).

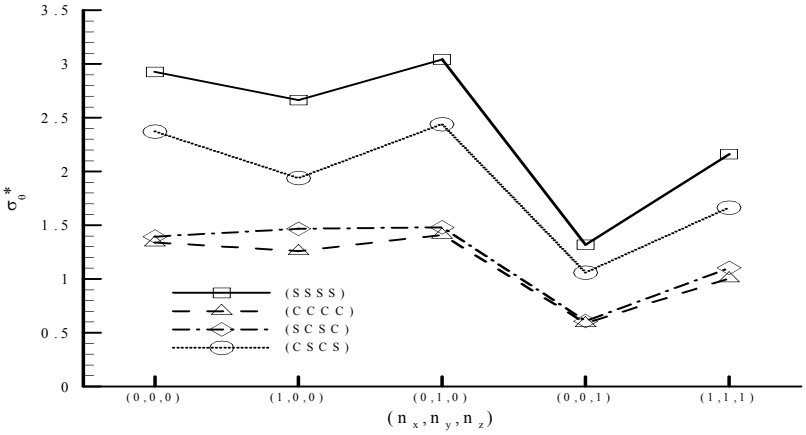

Fig.23
The effect of boundary conditions on non-dimensional stress σ_θ^*. ($a_0 = 0.2$, a = 0.8, $\theta_0 = \pi / 3$, z = 0.1, $q = 10^3$, $K_0 = J_0 = 0$, $Tu = T_1 = 0$).

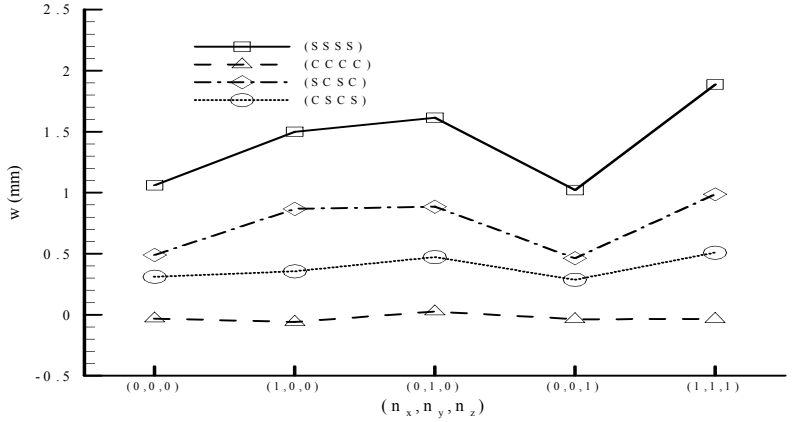

Fig.24
The effect of boundary conditions on the deflection w. ($a_0 = 0.2$, a = 0.8, $\theta_0 = \pi / 3$, z = 0.1, q = 0, $K_0 = J_0 = 0$, Tu =300, T_1=0).

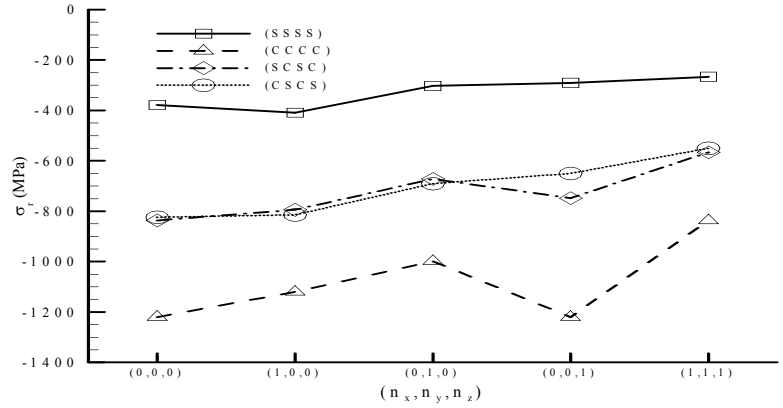

Fig.25
The effect of boundary conditions on the stress σ_r . ($a_0 = 0.2$, a = 0.8, $\theta_0 = \pi / 3$, z = 0.1, q = 0, $K_0 = J_0 = 0$, Tu = 300, T_1= 0).

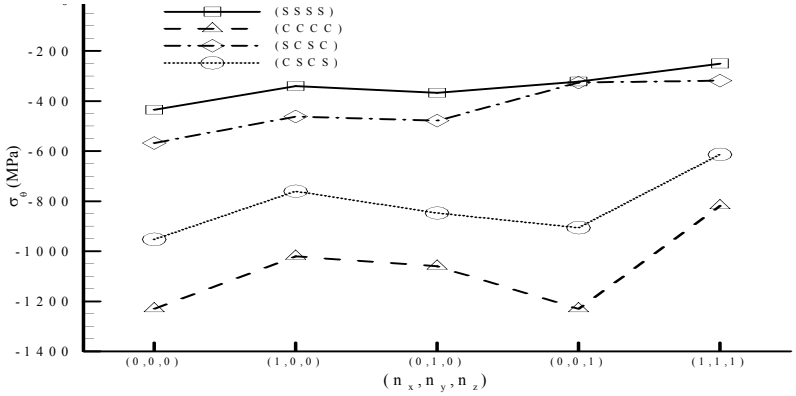

Fig.26
The effect of boundary conditions on non-dimensional stress σ_θ . ($a_0 = 0.2$, a = 0.8, $\theta_0 = \pi / 3$, z = 0.1, q = 0 , $K_0 = J_0 = 0$, Tu = 300 ,T_1 = 0).

As previously mentioned, the deformation of the plate under mechanical and thermal loading utilized in this study differs from one another. To provide a better understanding of the deformation behavior and the distribution of stress at various points on the plate, Fig. 27 is presented. This figure illustrates the deformation of the lower surface of the plate, as well as the radial and circumferential stresses on both the upper and lower surfaces for different material distributions. As observed, the deformations and stresses resulting from thermal loading exhibit more complex distribution. Furthermore, according to Fig. 27, although the deformation and stress distribution are largely dependent on the geometry of the plate, different material distributions lead to variations in these aspects. It is also noted that the changes in stresses occur more gradually from one point to another in the plate under mechanical

loading, while for the plate under thermal loading, particularly near the edges, sudden changes in stress magnitude are observed

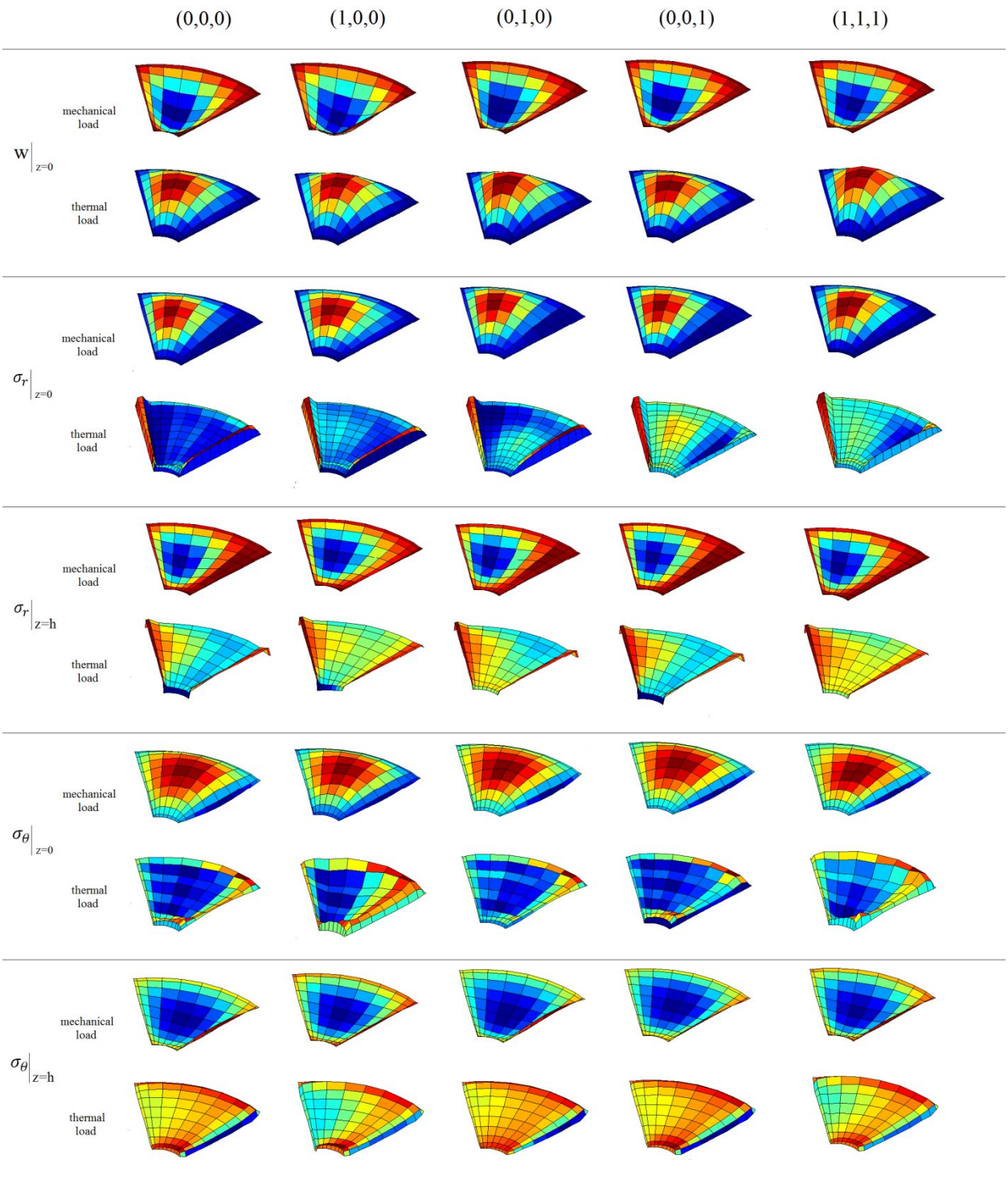

Fig.27
The effect of material distribution on the deflection and stresses.

6 CONCLUSIONS

In this research, the bending of annular sector plates made from multi-directionally functionally graded materials under mechanical and thermal loads is investigated for the first time using Generalized Differential Quadrature (GDQ). The study also examines the effects of boundary conditions and the placement of the plate on an elastic foundation on the resulting deformations and stresses. New graphs and tables presenting results in this area are displayed for the first time.

The results showed that variations in the material composition of the plate in different directions of cylindrical coordinates can have varying degrees of impact on the deformation and stresses of the plate.

The results indicated that the presence of the elastic foundation with any coefficient K_0 and J_0 can reduce the deformation of all five types of plates, with an increase in K_0 proving to be more effective than J_0 for the plate under mechanical load throughout the studied range. In contrast, under thermal loading, the opposite is observed. Additionally, the elastic foundation leads to a decrease in radial and circumferential stress values across all plates. Within the examined range, the results indicated that increasing the angle of the sector leads to a reduction in both the deformation at the center of the plate and the radial stress at the designated point for the plate under mechanical load. For the plate under thermal load different behavior was observed.

The Results demonstrated that maximum and minimum deformations occur for the boundary conditions SSSS and CCCC, respectively. Studying the SCSC and CSCS boundary conditions indicate that, under mechanical loading, the curved edges have a more significant influence on the plate's behavior compared to the other edges. In contrast, under thermal loading, the opposite is observed.

The Results showed that while the deformation and stress distribution are primarily influenced by the plate's geometry, variations in material distribution also result in changes to these characteristics. It is important to note that stress changes occur more gradually from one point to another in the plate subjected to mechanical loading. In contrast, for the plate under thermal loading, especially near the edges, abrupt changes in stress magnitude are observed.

REFERENCES

[1] P. Van Vinh, M. Avcar, M.O. Belarbi, A. Tounsi, A new higher-order mixed four-node quadrilateral finite element for static bending analysis of functionally graded plates, Structures, 47, 1595-1612 (2023).
[2] E. Jomehzadeh, A. Saidi, S.R. Atashipour, An analytical approach for stress analysis of functionally graded annular sector plates, Materials & design, 30(9), 3679-3685 (2009).
[3] A. Saidi, E. Jomehzadeh, S. R. Atashipour, Exact analytical solution for bending analysis of functionally graded annular sector plates, International Journal of Engineering, Transactions A: Basics, 22(3), 307-316 (2009).
[4] F. Fallah, A. Nosier, Thermo-mechanical behavior of functionally graded circular sector plates, Acta Mechanica, 226(1), 37-54 (2015).
[5] M.H. Karimi, F. Fallah, Analytical non-linear analysis of functionally graded sandwich solid/annular sector plates, Composite Structures, 275,114420 (2021).
[6] M. Aghdam, N. Shahmansouri, M. Mohammadi, Extended kantorovich method for static analysis of moderately thick functionally graded sector plates, Mathematics and Computers in Simulation, 86, 118-130 (2012).
[7] M. Golmakani, M. Kadkhodayan, Large deflection thermoelastic analysis of functionally graded stiffened annular sector plates, International Journal of Mechanical Sciences, 69, 94-106 (2013).
[8] M. Golmakani, J. Alamatian, Large deflection analysis of shear deformable radially functionally graded sector plates on two-parameter elastic foundations, European Journal of Mechanics-A/Solids, 42, 251-265 (2013).
[9] A. Fereidoon, Bending analysis of functionally graded annular sector plates by extended Kantorovich method, Composites Part B: Engineering, 43(5), 2172-2179 (2012).
[10] F. Alinaghizadeh, M. Shariati, Geometrically non-linear bending analysis of thick two-directional functionally graded annular sector and rectangular plates with variable thickness resting on non-linear elastic foundation, Composites Part B: Engineering, 86, 61-83 (2016).
[11] F. Alinaghizadeh, M. Shariati, Static analysis of variable thickness two-directional functionally graded annular sector plates fully or partially resting on elastic foundations by the GDQ method, Journal of the Brazilian Society of Mechanical Sciences and Engineering, 37, 1819-1838 (2015).
[12] S.M. Mousavi, M. Tahani, Analytical solution for bending of moderately thick radially functionally graded sector plates with general boundary conditions using multi-term extended Kantorovich method, Composites Part B: Engineering, 43(3), 1405-1416 (2012).

[13] F. Alinaghizadeh, M. Kadkhodayan, Large deflection analysis of moderately thick radially functionally graded annular sector plates fully and partially rested on two-parameter elastic foundations by GDQ method, Aerospace Science and Technology, 39, 260-271 (2014).
[14] F. Alinaghizadeh, M. Kadkhodayan, Investigation of nonlinear bending analysis of moderately thick functionally graded material sector plates subjected to thermomechanical loads by the GDQ method, Journal of Engineering Mechanics, 140(5), 04014012 (2014).
[15] F. Fallah, M. Karimi, Non-linear analysis of functionally graded sector plates with simply supported radial edges under transverse loading, Mechanics of Advanced Composite Structures, 6(1), 65-74 (2019).
[16] F. Fallah, A. Khakbaz, On an extended Kantorovich method for the mechanical behavior of functionally graded solid/annular sector plates with various boundary conditions, Acta Mechanica, 228(7), 2655-2674 (2017).
[17] M. Kadkhodayan, M.E. Golmakani, Non-linear thermo-mechanical bending behavior of thin and moderately thick functionally graded sector plates using dynamic relaxation method, International Journal of Engineering, 29(6), 870-878 (2016).
[18] H. Zafarmand, M. Kadkhodayan, Three dimensional elasticity solution for static and dynamic analysis of multi-directional functionally graded thick sector plates with general boundary conditions, Composites Part B: Engineering, 69, 592-602 (2015).
[19] K. Asemi, M. Salehi, M. Sadighi, Three dimensional static and dynamic analysis of two dimensional functionally graded annular sector plates, Structural Engineering And Mechanics: An International Journal, 51(6), 1067-1089 (2014).
[20] M. Livani, Three dimensional bending analysis of multi-directional functionally graded annular sector thick plates, Aerospace Knowledge and Technology Journal, 9(1), 113-124 (2020).
[21] M.J. Niaraki, H.Torabian, B. Abbaripour, A numerical solution of a circular section made of functionally graded material (FGM) under a transverse load, with a simple support on the radial Edges, Journal of Technology in Aerospace Engineering, 3(1), 31-40 (2019).
[22] G. Reddy, An investigation into the numerical analysis of refined higher order shear deformation theory for frequency responses of two-directional functionally graded taper beams, Journal of Computational Applied Mechanics, (2024).
[23] P.S. Ghatage, V.R. Kar, P.E. Sudhagar, On the numerical modelling and analysis of multi-directional functionally graded composite structures: A review, Composite Structures, 236, 111837 (2020).
[24] M.M. Alipour, M. Shariyat, Stress analysis of two-directional FGM moderately thick constrained circular plates with non-uniform load and substrate stiffness distributions, Journal of Solid Mechanics, 2(4), 316-331(2010).
[25] C. Lü, C.W. Lim, W. Chen, Semi□analytical analysis for multi□directional functionally graded plates: 3□D elasticity solutions, International Journal for Numerical Methods in Engineering, 79(1), 25-44 (2009).
[26] M. Adineh, 2024, Natural frequency analysis of multi-directional functionally graded rectangular plates on elastic foundation using three-dimensional elasticity theory, Mechanic of Advanced and Smart Materials, 4(1), 40-63 (2024).
[27] M. Adineh, H. Estiri, Effect of temperature on the natural frequency of multi-directional functionally graded rectangular plates on an elastic foundation using three-dimensional elasticity theory, Contributions of Science and Technology for Engineering, 2(4), 13-27(2025).
[28] C.W. Bert, M. Malik, Differential Quadrature Method in Computational Mechanics: A Review, (1996).
[29] M. Aghdam, M. Mohammadi, V. Erfanian, Bending analysis of thin annular sector plates using extended Kantorovich method, Thin-Walled Structures, 45(12), 983-990 (2007).
[30] H.-T.Thai, D.-H. Choi, A refined plate theory for functionally graded plates resting on elastic foundation, Composites Science and Technology, 71(16), 1850-1858 (2011).
[31] M. Adineh, M. Kadkhodayan, Three-dimensional thermo-elastic analysis of multi-directional functionally graded rectangular plates on elastic foundation, Acta Mechanica, 228, 881-899 (2017).